AMERICAN ACADEMY OF OPHTHALMOLOGY®

Analysis of Progressive Neovascularization in Diabetic Retinopathy Using Widefield OCT Angiography

Akihiko Shiraki, MD,[1] *Susumu Sakimoto, MD, PhD,*[1,2] *Mami Eguchi, MD,*[1] *Masanori Kanai, MD,*[1] *Chikako Hara, MD, PhD,*[1] *Yoko Fukushima, MD, PhD,*[1,2] *Kentaro Nishida, MD, PhD,*[1] *Ryo Kawasaki, MD, MPH, PhD,*[1] *Hirokazu Sakaguchi, MD, PhD,*[1] *Kohji Nishida, MD, PhD*[1,2]

Purpose: To document enlarged neovascularization elsewhere (NVE) quantitatively and morphologically using widefield swept-source (SS) OCT angiography (OCTA) with vitreoretinal interface (VRI) slab images.

Design: Retrospective, observational imaging study.

Participants: The study included 46 NVE examples in 25 eyes of 21 consecutive patients who demonstrated severe proliferative diabetic retinopathy with NVE between March 2018 and June 2020 at Osaka University Hospital.

Methods: All patients underwent ophthalmologic examination, including ultra-widefield fluorescein angiography and widefield SS OCTA scans.

Main Outcome Measures: We evaluated the area and the vascular density (VD) of NVE lesions detected on five 12 × 12-mm^2 or two 15 × 9-mm^2 SS OCTA panoramic VRI slab images obtained at the first and final visits.

Results: At baseline, the mean NVE area on OCTA was 1.85 ± 2.81 mm^2, and the VD of the NVE lesions was 73.9 ± 14.6%. At the final visit, the mean NVE area on OCTA was 2.14 ± 3.14 mm^2, and the mean VD of the NVE lesions was 65.3 ± 17.1%. The average NVE size change (square millimeters per month) was associated significantly with the ischemic index ($P = 0.009$). Growth of NVE area was classified into 2 patterns: round (61.8%) and ramified (38.2%). The round group tended to have a larger ischemic index at baseline than the ramified group ($P = 0.0375$).

Conclusions: We quantified the size and density of NVE lesions over time. The NVE size increase was associated significantly with the severity of ischemic changes. Furthermore, the round growth pattern was correlated significantly with the ischemic index. These findings suggest that the morphologic features of NVE are associated with more severe ischemia. *Ophthalmology Retina 2021;■:1–8 © 2021 by the American Academy of Ophthalmology. This is an open access article under the CC BY-NC-ND license (http://creativecommons.org/licenses/by-nc-nd/4.0/).*

Supplemental material available at www.ophthalmologyretina.org.

Proliferative diabetic retinopathy (PDR) is a severe complication of diabetes mellitus, which is the main cause of vision loss and blindness during working age in developed countries.[1,2] The main features of PDR are a large nonperfused area (NPAs) and neovascularization, the latter of which is projected on the internal limiting membrane (ILM). It is important to diagnose PDR in the early stages to maintain visual acuity and to perform panretinal photocoagulation (PRP) with or without vitreous injection of anti–vascular endothelial growth factor (VEGF) agents to prevent disease progression.

Fluorescein angiography (FA) is the standard procedure to evaluate the severity of diabetic retinopathy. Fluorescein angiography detects NPAs, intraretinal microvascular abnormalities, and neovascularization.[3] However, FA is burdensome, requires intravenous injection, and carries the risk of systemic adverse reactions.[4] In particular, neovascularization shows characteristics of irregular vessel structure and high leakage on FA. Namely, FA provides limited detailed characterization of neovascularization and the surrounding retinal microvasculature because the area is obscured rapidly by the leakage of fluorescein dye, and only 1 eye can be chosen for characterization in the early transit stage.[5]

In contrast, OCT angiography (OCTA) can facilitate the visualization of the retinal vessel structures noninvasively and repeatably.[6] Unlike FA, OCTA does not involve dye leakage, and it enables the acquisition of 3-dimensional information with relatively high axial resolution.[7,8] Previous studies using spectral-domain OCTA demonstrated that the morphologic features of neovascularization depend on the severity of PDR; however, those OCTA scans

https://doi.org/10.1016/j.oret.2021.05.011
ISSN 2468-6530/21

allowed visualization of a limited area.[9,10] Furthermore, the newly developed swept-source (SS) OCTA (PLEX Elite 9000; Carl Zeiss Meditec, Dublin, CA) obtains larger images, which are similar to a montage of widefield OCTA images.[8] Boundary-specific segmentation technologies can depict the specific vasculature of each retinal layer, including the superficial and deep plexus mode, outer retina mode, avascular layer mode, choriocapillaris, or choroid, using en face angiography. OCT angiography also provides cross-sectional B-scans that are useful for detecting pathologic lesions of the vitreoretinal interface caused by vitreous traction.[7,8,11,12] Combining these techniques has enabled the performance of OCTA with installation of vitreoretinal interface (VRI) slabs to visualize the morphologic features of retinal neovascularization.[5,13] Recently, SS OCTA VRI slab images were reported to be comparable with those of FA for detecting neovascularization in PDR.[13,14] However, few studies have reported detailed morphologic findings or have quantified the regression or progression of neovascularization using widefield OCTA images. Therefore, in this study, we evaluated and quantified enlarged neovascularization elsewhere (NVE) lesions in eyes with PDR over time using widefield SS OCTA images.

Methods

Study Population and Data Collection

We retrospectively reviewed patients with PDR who underwent ultra-widefield (UWF) FA and widefield SS OCTA scans between March 2018 and June 2020 at Osaka University Hospital. This study was performed in accordance with the tenets of the Declaration of Helsinki, and all patients provided informed consent. Institutional review board/ethics committee approval was obtained in Osaka University Hospital.

All patients underwent the following eye examinations: UWF fundus photography, UWF FA, widefield SS OCTA, slit-lamp examination, detailed funduscopy, and hemoglobin A1c (HbA1c) blood testing. Any medical history of hypertension was noted. Proliferative diabetic retinopathy with neovascularization was diagnosed based on a comprehensive ophthalmologic examination comprising slit-lamp examination, UWF funduscopy, and UWF FA. The follow-up period in this study was defined as the time between each patient's baseline and final OCTA scans (Table 1).

Table 1. Demographic and Ocular Characteristics of the Study Population

Parameter	Data	P Value
No. of patients	21	
No. of eyes	25	
No. NVE lesions	46	
Age (yrs), mean ± SD	51.0 ± 13.6	
Sex, no. (%)		
Male	16 (76.2)	
Female	5 (23.8)	
Type of DM, no. (%)		
2	21 (100)	
1	0 (0)	
HbA1c level (%), mean ± SD	7.97 ± 1.56	
Blood pressure (mmHg)		
Systolic		
Mean ± SD	130 ± 20	
Range	98–165	
Diastolic		
Mean ± SD	75 ± 13	
Range	52–108	
Duration of follow-up (mos)		
Mean ± SD	4.84 ± 3.04	
Range	2–13	
Area of NVE lesions (mm^2)		
Baseline		0.0088
Mean ± SD	1.85 ± 2.81	
Range	0.01–13.5	
Final		
Mean ± SD	2.14 ± 3.14	
Range	0.07–16.2	
Vascular density of NVE lesions (%)		
Baseline		0.0002
Mean ± SD	73.9 ± 14.6	
Range	42.0–100.0	
Final		
Mean ± SD	65.3 ± 17.1	
Range	25.5–100.0	

DM = diabetes mellitus; HbA1c = hemoglobin A1c; NVE = neovascularization elsewhere; SD = standard deviation.

OCT Angiography Scans

For all patients, OCTA images were acquired during at least 2 visits using the SS OCT PLEX Elite 9000. Either five 12 × 12-mm^2 or two 15 × 9-mm^2 SS-based widefield OCTA montage scans were performed. Regarding OCTA scans using the Plex Elite with an optical resolution limit of 20 μm, the standard 12 × 12-mm Angio scan has a sampling of 500 × 500 A-scans (sample spacing, 24 μm), and the 15 × 9-mm scan has a sampling of 834 × 500 A-scans (sample spacing, 18 μm). Areas of NVE were detected in each VRI slab, although most of the OCTA images included segmentation errors (Fig 1B, C). All B-scan lines in the OCTA images were corrected manually, and the NVE lesions were delineated clearly in each VRI slab (Fig 1D, E). The outline of NVE lesions was defined by manual delineation (performed by A.S. and S.S.). The sum of pixels surrounded by the outline of the NVE lesion was converted from pixels to square millimeters, which is defined as the area of NVE.[13] Image quality exceeding eight tenths of the signal strength determined using OCTA equipment and software was defined as high quality. Those with less than seven tenths of the signal strength were defined as low-quality images and were excluded from the current analyses.

OCT Angiography Image Analysis

Two of the authors (A.S. and S.S.) measured the area and vascular density (VD) of each NVE lesion based on the OCTA images, and the nonperfusion area was measured via UWF FA scans. The NVE images were cropped from the OCTA VRI slab images using Photoshop (Adobe Systems, Inc., San Jose, CA) after correcting the segmentation errors as described above. The OCTA images captured by the Elite system were processed subsequently using ImageJ software (National Institutes of Health, Bethesda, MD; http://imagej.nih.gov/ij/) with the same pixel densities. Each NVE area was measured using Image J software as well. For convenience, each NVE area was converted from pixels to square millimeters based on the original 12 × 12-mm^2 or 15 × 9-mm^2 image size. The measurement of the VD of the NVE lesion was performed based on a previous report.[15] Briefly, we converted OCTA images into 8 bits and assigned a value of 255 (completely white)

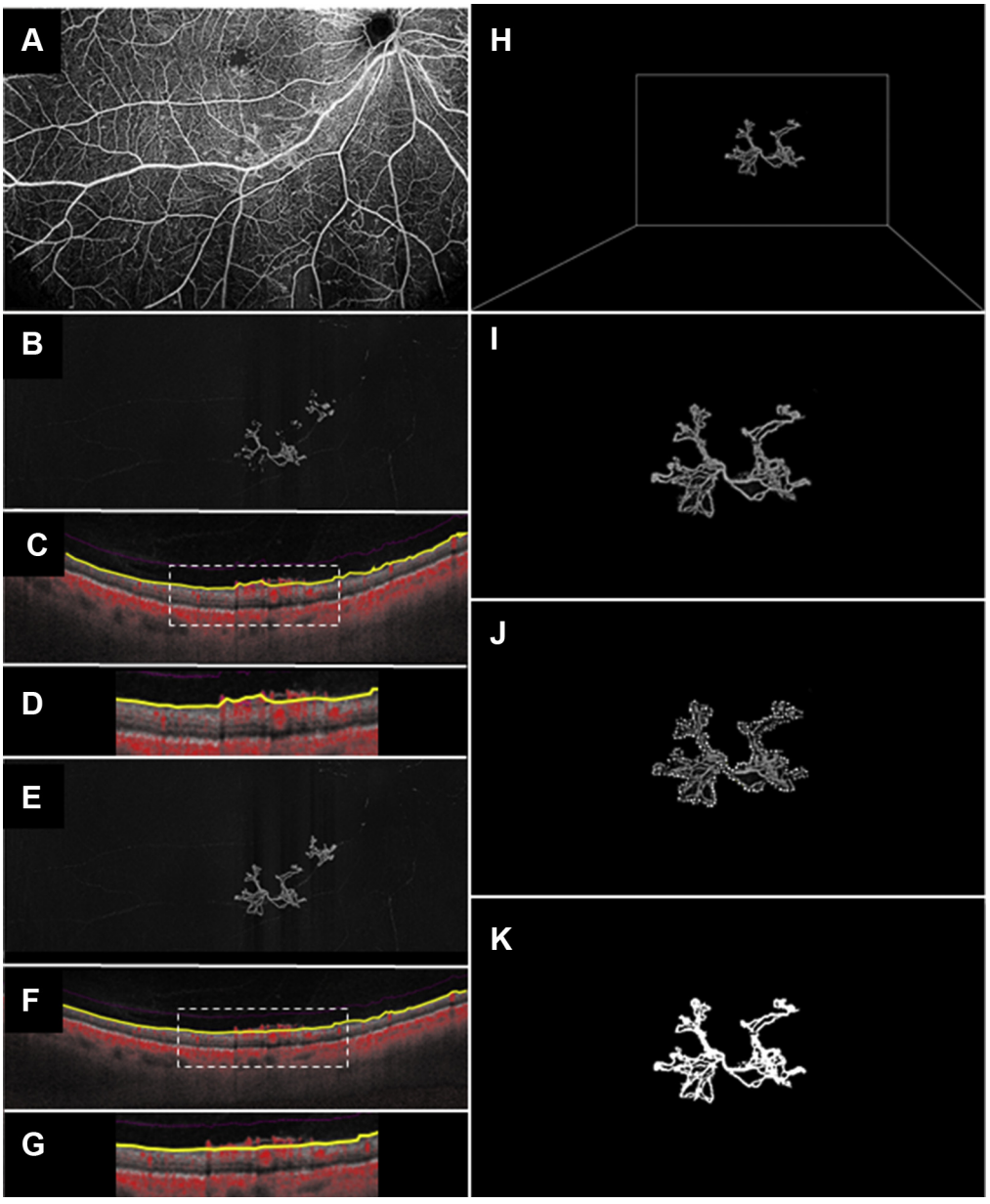

Figure 1. Quantitative analysis of neovascularization elsewhere (NVE) lesions as shown in en face OCT angiography (OCTA) images. **A**, **B**, En face OCTA images showing the deep and superficial vessels of the retina, but only a partial portion of the NVE lesion because of a segmentation error: (**A**) en face OCTA image of the total retina slab and (**B**) the vitreoretinal interface (VRI) slab based on automated VRI segmentation. **C**, **D**, **E**, Automated VRI detection showing an incomplete NVE structure resulting from a segmentation error: (**C**) B-scan image with flow dots showing automated VRI segmentation (yellow line) and (**D**) magnified image of the area within the dotted white square in (**C**). **F**, **G**, **H**, Manual correction of VRI segmentation clarifies the structure of NVE lesions: (**F**) B-scan image with flow dots showing manual VRI segmentation (yellow line) and (**G**) magnified image of the area within the dotted white square in (**F**). **H**, **I**, Identification of a targeted NVE lesion: (**I**) high magnification of the cropped image of the white square shown in (**H**). **J**, Quantification of the area of the NVE with cropped OCTA images. **K**, Density analysis of the NVE using the binary image shown in (**H**).

to all pixels with a positive grey level and a value of 0 (completely black) to the others using the Otsu Auto Local Threshold method (radius, 75 pixels; parameter, 1 [default]). Using the binary image, the VD was calculated as the mean of all of the white pixels of the NVE, and the VD of the NVE lesions (percentage) was expressed as: VD / NVE area $\times$ 100. Thus, a decrease in the number of vessels in the same NVE lesion is reflected by a decrease in the flow signals at an examined area, which can be interpreted as a decrease in the VD of the area. The NVE lesion size change or the VD change per month was calculated using the fraction of the difference between the baseline and final OCTA scans, which was divided subsequently by the follow-up period. Based on the comparison of the baseline and final NVE areas, expanding NVE lesions were defined as those that had increased to more than 1.05 times that of the baseline values (final NVE area / baseline NVE area). Shrinking NVE lesions were defined as those whose final areas were less than 0.95 times that of the baseline values.

The morphologic types of the NVE lesions were classified as predominantly round or ramified. When an NVE lesion exhibited characteristics of both types at different parts of the lesion, it was classified based on the predominant shape observed. The eyes were classified further based on the predominant type of NVE lesions they contained, with the more obviously round or ramified NVE lesions chosen for inclusion in the study. If an eye contained only round or ramified NVE lesions, it was classified as round or ramified, respectively. However, if an eye contained both types of NVE lesions, it was classified according to the majority type. For example, if an eye had 1 round and 2 ramified NVE lesions, the eye was classified as predominantly ramified. If the numbers of each NVE type were the same in both eyes, the classification was based on whichever NVE lesion was the largest. Classification of the developing NVE lesions was determined by 2 of the authors (A.S. and S.S.). Any disagreement between the 2 graders was resolved by another retina specialist (M.E.).

Widefield Fluorescein Angiography

Ultra-widefield FA images were obtained using an Optomap panoramic 200Tx imaging system (Optos, PLC, Dunfermline, United Kingdom). All patients underwent FA according to a standard protocol after intravenous injection of 10% sodium. An NVE lesion of PDR was diagnosed based on indirect ophthalmoscopy UWF imaging findings and the presence of fluorescent leakage from a new vessel in UWF FA. Calculation of the ischemic index was based on methods published elsewhere.[16,17] Briefly, the NPA and the total UWF imaging area were measured using ImageJ software. Subsequently, the ischemic index in this study was calculated as the proportion of the NPA to the total UWF imaging area.

Statistical Analysis

Data were analyzed using GraphPad Prism (GraphPad Software, La Jolla, CA). A one-way analysis of variance and univariate regression were used to investigate the associations among NVE lesion size, density change, and other parameters such as age, HbA1c levels, ischemic index at baseline, photocoagulation between examinations, and the presence of adjacent NPAs. The Mann−Whitney *U* test and paired *t* test also were performed, as appropriate. *P* values of less than 0.05 were considered statistically significant.

Results

Patient Characteristics

In total, we analyzed 46 NVE lesions (25 eyes of 21 patients; 16 men and 5 women). The mean patient age was 51.0 ± 13.6 years (range, 33−79 years), and the mean duration of the follow-up period—namely, the term between 2 OCTA examinations—was 4.84 ± 3.04 months (range, 2−13 months). At baseline, the mean area of NVE on OCTA was 1.85 ± 2.81 mm^2 (range, 0.01−13.5 mm^2), and the mean VD of NVE was 73.9 ± 14.6% (range, 42.0−100.0%). At the final visit, the mean NVE area on OCTA was 2.14 ± 3.14 mm^2 (range, 0.07−16.2 mm^2), and the mean VD of the NVE lesion was 65.3 ± 17.1% (range, 25.5−100.0%). Of 25 eyes, 3 were treatment naïve and subsequent PRP was initiated (12.0%); additional photocoagulation was performed in 11 eyes (44.0%), whereas no additional treatment was needed in 11 eyes (44.0%).

Table 2. Separate Regression Analysis for the Association between Neovascularization Elsewhere Lesion Size and Density Change

Parameter	R^2 Value	*P* Value
Age		
NVE size change (mm^2/mo)	0.008333	0.5463
NVE density change (%/mo)	0.05213	0.127
HbA1c level		
NVE size change (mm^2/mo)	0.00243	0.7449
NVE density change (%/mo)	0.02854	0.2617
Ischemic index at baseline		
NVE size change (mm^2/mo)	0.09033	0.0424
NVE density change (%/mo)	0.05312	0.1233

HbA1c = hemoglobin A1c; NVE = neovascularization elsewhere.

Table 2 shows the comparison and separate regression analysis for the association between NVE lesion size and density change. We evaluated the correlation between age, HbA1c levels, the ischemic index, and the following elements: NVE lesion size change per month and the NVE lesion density change per month. The ischemic index at baseline showed a significant association with the average NVE lesion size change (square millimeters per month). Comparison of the baseline and final areas of the 46 NVE lesions revealed that 34 had become more than 1.05 times larger at the time of the final OCTA scan compared with the baseline OCTA measurements (expanding NVE lesions). Seven NVE lesions were between 0.95 and 0.105 times larger, and 5 NVE lesions (1 of 5 NVE lesions had received anti-VEGF treatments via intravitreal injection) were less than 0.95 times smaller at the final OCTA scan relative to the size at baseline (shrinking NVE lesions).

We subsequently analyzed the 34 expanding NVE lesions that had grown more than 1.05 times larger and noted that the enlargement of the NVE lesions could be classified into 2 patterns: round and ramified (Fig 2). The 34 expanding NVE lesions did not receive intravitreal anti-VEGF treatment. In the round pattern group, the spread centered around the vein; in the ramified pattern group, it extended straight from the tip of the NVE. Of the 34 NVE lesions, 21 constituted the round group (61.8%) and 13 constituted the ramified group (38.2%; Table 3). The NVE area at baseline did not differ between the round (1.18 ± 1.40 mm^2) and ramified (2.10 ± 2.99 mm^2; $P = 0.2354$) patterns. Similarly, the NVE area at the final visit did not differ between the groups (1.61 ± 1.73 mm^2 in the round group and 2.57 ± 3.61 mm^2 in the ramified group; $P = 0.3016$). Neither the NVE lesion size change (square millimeters per month) nor the NVE density change (percentage per month) were different between the 2 groups ($P = 0.7523$ and $P = 0.3778$); however, the density of NVE lesions (percentage) at baseline and at the final OCTA examination were significantly higher in the round group than in the ramified group ($P = 0.0449$ and $P = 0.0117$, respectively). The number of round-dominant eyes was 13 (61.9%), and the number of ramified-dominant eyes was 8 (38.1%). No differences were found between the round and ramified groups in terms of age, HbA1c level, or photocoagulation number; however, a significant difference was found in the ischemic index at baseline. The ischemic index at baseline of the

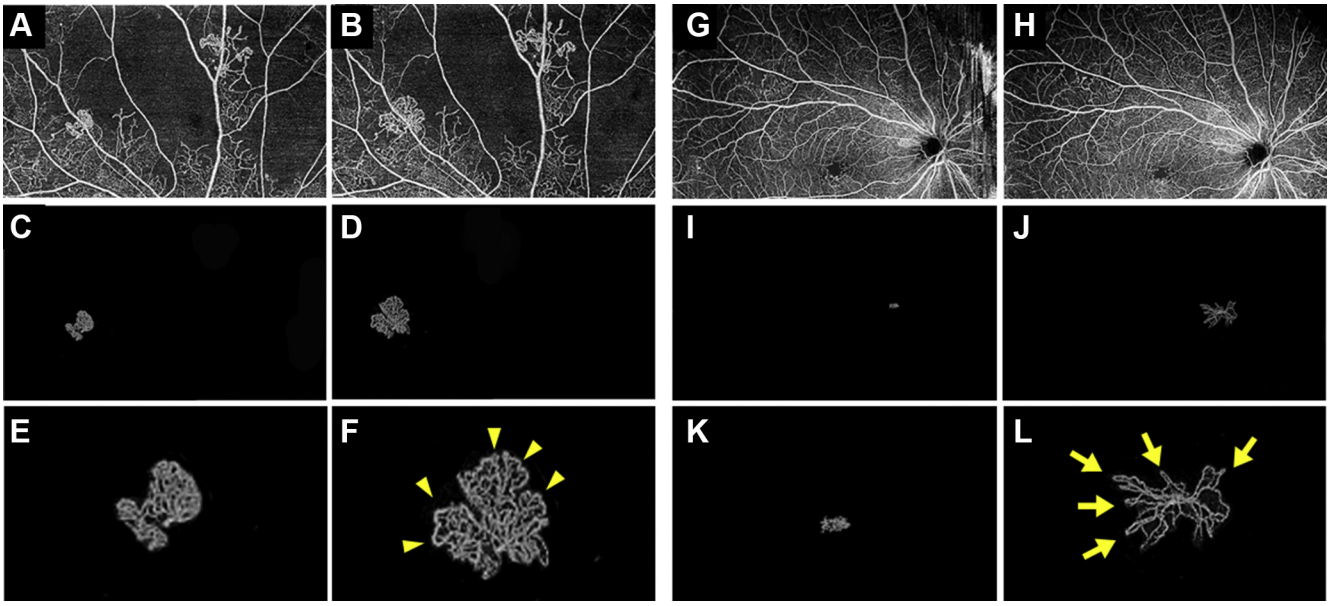

Figure 2. Two types of neovascularization elsewhere (NVE) lesion progression. **A**, **B**, En face OCT angiography (OCTA) images of the round type of NVE lesion spreading in all directions from the original vein at (**A**) baseline and (**B**) the final visit. **C**, **D**, Neovascularization elsewhere lesions isolated using the manual vitreoretinal interface (VRI) technique, cropped from (**A**) and (**B**), respectively. **E**, **F**, High-magnification images of NVE lesions in (**E**) and (**F**), respectively. Yellow arrowheads indicate spreading vasculature. **G**, **H**, En face OCTA images of the ramified type of NVE lesion extending its tips from the original vein at (**G**) baseline and (**H**) the final visit. **I**, **J**, Neovascularization elsewhere lesions isolated using the manual VRI technique, cropped from (**G**) and (**H**), respectively. **K**, **L**, High magnification of NVE lesions in (**E**) and (**F**), respectively. Yellow arrows indicate dendritically extending vascular tips.

round-dominant eyes was higher than that of the ramified-dominant eyes (86.4 ± 6.4 and 79.3 ± 12.7, respectively; $P = 0.0375$).

Supplemental Table 1 (available at www.ophthalmologyretina.org) shows the changes in area (square millimeters) and VD of each NVE lesion. The mean NVE area increased overall ($P = 0.0088$). In the group of eyes that received photocoagulation, the mean area at the final scan had increased significantly from that at baseline ($P = 0.0129$). In the group of eyes that did not receive photocoagulation, no significant difference was found between values at baseline and at the final scan ($P = 0.2292$). The mean VD of NVE lesions decreased significantly overall ($P = 0.0002$), in the photocoagulation group ($P = 0.0366$), and in the nonphotocoagulation group ($P = 0.0018$).

Discussion

Pathologic angiogenesis is linked to eye diseases such as PDR and age-related macular degeneration, as well as to cancer, psoriasis, and endometriosis.[18] We believe our methods of isolation and quantification are key in the attempt to measure a speed or density change during the development of microvasculature in pathologic angiogenesis. In this study, using VRI imaging techniques in widefield OCTA, we succeeded in isolating and visualizing NVE lesions, and our method enabled us to quantify the development of NVE lesions in PDR. The NVE area increased, allowing us to examine the factors affecting the speed of NVE lesion development. Indeed, the NVE lesion size change was correlated significantly with a larger NPA. Among these enlarged NVE lesions, a round, but not a ramified, morphologic feature was associated significantly with a larger ischemic index of the retina. These findings suggest that the morphologic features of the NVE can predict the degree of ischemia in PDR. Namely, when NVE lesions in an eye with PDR grow in a round shape, we refer patients for an internal medicine consultation and encourage frequent ophthalmic check-ups.

The OCTA VRI results contained some false-negative images resulting from segmentation errors at the ILM level (Fig 1A–C). Segmentation errors have been recognized as a major source of artifacts in OCTA images of the eyes of patients with diabetes mellitus.[19,20] Manual correction of the segmentation as performed in this study is a potential solution to this issue.[20] In fact, after manually correcting the segmentation, the sensitivity of the VRI slab images for detecting neovascularization increased from 73% to 84%.[13] This shows that the efficacy of widefield SS OCTA VRI slab images for detecting neovascularization in PDR was comparable with that of FA, which has a sensitivity of 73%. This technique enabled us to visualize NVE lesions clearly and subsequently to quantify the size and density of each.

However, the VD of NVE lesions decreased during follow-up in this study. The reason for the VD decrease was unclear; however, our results imply that when an NVE becomes larger, its density becomes smaller. Another possible reason for the VD decrease is that initial or additional photocoagulation was performed in 56.0% of eyes during

Table 3. Pattern of Neovascularization Elsewhere Lesion Development and Its Associated Factors

Classification	Round	Ramified	*P* Value
No. of NVE lesions (%)	21 (61.8)	13 (38.2)	
Area of NVE lesions (mm^2)			
Baseline			0.2354
Mean ± SD	1.18 ± 1.40	2.10 ± 2.99	
Range	0.01–4.47	0.08–11.3	
Final			0.3016
Mean ± SD	1.61 ± 1.73	2.57 ± 3.61	
Range	0.07–6.12	0.40–14.1	
NVE size change (mm^2/mo)			0.7523
Mean ± SD	0.10 ± 0.12	0.12 ± 0.25	
Range	0.00–0.413	0.00–0.92	
Vascular density of NVE lesions (%)			
Baseline			0.0449
Mean ± SD	78.0 ± 13.8	68.3 ± 12.0	
Range	47.2–100.0	49.0–95.7	
Final			0.0117
Mean ± SD	70.8 ± 14.2	56.1 ± 17.8	
Range	37.4–100.0	25.5–80.4	
NVE density change (%/mo)			0.3778
Mean ± SD	−1.76 ± 6.16	−3.48 ± 4.03	
Range	−12.1 to 20.0	−10.7 to 3.44	
Age (yrs), mean ± SD	54.9 ± 13.6	49.0 ± 15.6	0.4451
HbA1c level (%), mean ± SD	7.85 ± 1.47	8.14 ± 2.06	0.7346
PC received, no. of NVE lesions (%)	11 (52.4)	7 (53.8)	0.9999
Ischemic index at baseline, mean ± SD	86.4 ± 6.4	79.3 ± 12.7	0.0375

HbA1c = hemoglobin A1c; NVE = neovascularization elsewhere; PC = photocoagulation; SD = standard deviation.

follow-up. In a previous report that concluded that PRP contributed to the regression of NVE lesions, the authors used the parameter of "flow area," which is thought to be the sum of the total pixels of the NVE lesions.[9] In a prospective study, Russell et al[5] reported that 53% of patients regressed after PRP, whereas 47% were judged to have disease progression according to OCTA and FA results. In the current study, enlargement of the NVE areas could have occurred during certain periods, even after PRP, in the treatment-naïve eyes or after undergoing additional photocoagulation in the insufficiently performing eyes after PRP. Panretinal photocoagulation induces a regression of the flow in the NVE, leading to decreased VD. This simply could be the result of a time lag between the changes in the area and the VD of NVE lesions after photocoagulation. In addition, all eyes that had not been treated with photocoagulation already had undergone PRP; similar to what is observed during the creeping enlargement of photocoagulation scars, this previous PRP treatment could have led to advanced retinal atrophy, resulting in a decrease in the VD of the NVE lesions. Further studies are needed to clarify the mechanism.

The area of the UWF FA images in this study was larger than that of widefield OCTA images. However, widefield OCTA may be sufficient from a clinical standpoint because most NVE lesions in PDR are observed within the mid periphery of the retina, which is within the zone covered by widefield OCTA images.[14,21] Thus, it is rare for NVE lesions to be detected by UWF FA, but not by widefield OCTA.

This study did have some limitations. First, it was retrospective with a relatively small sample size. Some of the eyes received photocoagulation during follow-up because our study included eyes with severe PDR. It should be noted that ethical issues will increase when we design a prospective study to evaluate the natural course of NVE lesions. Second, it is technically impossible to distinguish neovascularization outside 300 μm of the ILM. Because of the machine's performance, the top of the VRI slab was set to 300 μm from the ILM surface. When a posterior vitreous detachment occurs, it is difficult to recognize all neovascularization because it may exceed the range of the VRI. Third, the performance of manual segmentation and measurements may limit the usefulness of these methods in day-to-day clinical settings, and further studies should include a more automated and objective way of assessing the correct morphologic features of NVE lesions. For example, Lu et al[22] reported that a portion of the NVE lesions went undetected and that this problem was associated with automated segmentation errors. Therefore, although time consuming, manual segmentation was necessary for most of the OCTA images to highlight the NVE lesions better.[14] Fourth, although we selected high signal-strength images, we did not perform a repeatability test in this study. Vessel density measurement especially in widefield images should acquire agreement and reliability of measurements that can be established in a future study. Further studies are needed to develop a more automated, clinician-friendly way of quantifying and segmenting NVE lesions.

In conclusion, by adopting VRI slab methods, we detected the size and density changes of NVE lesions. Furthermore, we classified NVE lesions based on round and ramified growth patterns. Further studies are needed to examine the relationship between the morphologic features and the severity of PDR. This study highlighted the importance of comprehensively evaluating the morphologic features, area, and VD of NVE lesions.

Footnotes and Disclosures

Originally received: December 12, 2020.
Final revision: April 27, 2021.
Accepted: May 13, 2021.
Available online: ■■■. Manuscript no. ORET-2020-983.

[1] Department of Ophthalmology, Osaka University Graduate School of Medicine, Osaka, Japan.

[2] Integrated Frontier Research for Medical Science Division, Institute for Open and Transdisciplinary Research Initiatives, Osaka University, Suita, Japan.

Presented in part at: American Academy of Ophthalmology Annual Meeting, November 2020, virtual meeting.

Disclosure(s):

All authors have completed and submitted the ICMJE disclosures form.

The author(s) have made the following disclosure(s): C.H.: Financial support - Menicon, Novartis, Bayer, Santen

R.K.: Financial support - Topcon, Office Future, Nanolux, Bayer, Novartis, Senju, Santen

HUMAN SUBJECTS: Human subjects were included in this study. The human ethics committees at Osaka University Hospital approved the study. All research adhered to the tenets of the Declaration of Helsinki. All participants provided informed consent.

No animal subjects were included in this study.

Author Contributions:

Conception and design: Shiraki, Sakimoto, Sakaguchi, Ko.Nishida

Analysis and interpretation: Shiraki, Sakimoto, Eguchi, Kawasaki

Data collection: Shiraki, Sakimoto, Eguchi, Kanai, Hara, Fukushima, Ke.Nishida, Kawasaki

Obtained funding: N/A

Overall responsibility: Sakimoto

Abbreviations and Acronyms:

FA = fluorescein angiography; **HbA1c** = hemoglobin A1c; **ILM** = internal limiting membrane; **NPA** = nonperfused area; **NVE** = neovascularization elsewhere; **OCTA** = OCT angiography; **PDR** = proliferative diabetic retinopathy; **PRP** = panretinal photocoagulation; **SS** = swept-source; **UWF** = ultra-widefield; **VD** = vascular density; **VEGF** = vascular endothelial growth factor; **VRI** = vitreoretinal interface.

Keywords:

Diabetic retinopathy, Neovascularization, OCT angiography.

Correspondence:

Susumu Sakimoto, MD, PhD, Department of Ophthalmology, Osaka University Graduate School of Medicine, Rm E7, 2-2 Yamadaoka, Suita, Osaka 565-0871, Japan. E-mail: susumu.sakimoto@ophthal.med.osaka-u.ac.jp.

References

1. Zhang X, Saaddine JB, Chou C-F, et al. Prevalence of diabetic retinopathy in the United States, 2005−2008. *JAMA*. 2010;304:649−656.
2. Early Treatment Diabetic Retinopathy Study Research Group. Classification of diabetic retinopathy from fluorescein angiograms. ETDRS report number 11. *Ophthalmology*. 1991;98:807−822.
3. Klein R, Klein BE, Moss SE. Epidemiology of proliferative diabetic retinopathy. *Diabetes Care*. 1992;15:1875−1891.
4. Kwiterovich KA, Maguire MG, Murphy RP, et al. Frequency of adverse systemic reactions after fluorescein angiography. Results of a prospective study. *Ophthalmology*. 1991;98:1139−1142.
5. Russell JF, Shi Y, Hinkle JW, et al. Longitudinal wide-field swept-source OCT angiography of neovascularization in proliferative diabetic retinopathy after panretinal photocoagulation. *Ophthalmol Retina*. 2019;3:350−361.
6. Spaide RF, Klancnik Jr JM, Cooney MJ. Retinal vascular layers imaged by fluorescein angiography and optical coherence tomography angiography. *JAMA Ophthalmol*. 2015;133:45−50.
7. Sakimoto S, Kawasaki R, Nishida K. Retinal neovascularization-simulating retinal capillary reperfusion in branch retinal vein occlusion, imaged by wide-field optical coherence tomography angiography. *JAMA Ophthalmol*. 2020;138:216−218.
8. Shiraki A, Sakimoto S, Tsuboi K, et al. Evaluation of retinal nonperfusion in branch retinal vein occlusion using wide-field optical coherence tomography angiography. *Acta Ophthalmol*. 2019;97:e913−e918.
9. Ishibazawa A, Nagaoka T, Yokota H, et al. Characteristics of retinal neovascularization in proliferative diabetic retinopathy imaged by optical coherence tomography angiography. *Invest Ophthalmol Vis Sci*. 2016;57:6247−6255.
10. Pan J, Chen D, Yang X, et al. Characteristics of neovascularization in early stages of proliferative diabetic retinopathy by optical coherence tomography angiography. *Am J Ophthalmol*. 2018;192:146−156.
11. Russell JF, Flynn Jr HW, Sridhar J, et al. Distribution of diabetic neovascularization on ultra-widefield fluorescein angiography and on simulated widefield OCT angiography. *Am J Ophthalmol*. 2019;207:110−120.
12. Sawada O, Ichiyama Y, Obata S, et al. Comparison between wide-angle OCT angiography and ultra-wide field fluorescein angiography for detecting non-perfusion areas and retinal neovascularization in eyes with diabetic retinopathy. *Graefes Arch Clin Exp Ophthalmol*. 2018;256:1275−1280.
13. Hirano T, Hoshiyama K, Hirabayashi K, et al. Vitreoretinal interface slab in OCT angiography for detecting diabetic retinal neovascularization. *Ophthalmol Retina*. 2020;4:588−594.
14. Pichi F, Smith SD, Abboud EB, et al. Wide-field optical coherence tomography angiography for the detection of proliferative diabetic retinopathy. *Graefes Arch Clin Exp Ophthalmol*. 2020;258:1901−1909.
15. Tsuboi K, Ishida Y, Kamei M. Gap in capillary perfusion on optical coherence tomography angiography associated with

persistent macular edema in branch retinal vein occlusion. *Invest Ophthalmol Vis Sci*. 2017;58:2038–2043.

16. Berry D, Thomas AS, Fekrat S, Grewal DS. Association of disorganization of retinal inner layers with ischemic index and visual acuity in central retinal vein occlusion. *Ophthalmol Retina*. 2018;2:1125–1132.
17. Sinova I, Rehak J, Nekolova J, et al. Correlation between ischemic index of retinal vein occlusion and oxygen saturation in retinal vessels. *Am J Ophthalmol*. 2018;188:74–80.
18. Folkman J. Angiogenesis. *Annu Rev Med*. 2006;57:1–18.
19. Spaide RF, Fujimoto JG, Waheed NK. Image artifacts in optical coherence tomography angiography. *Retina*. 2015;35:2163–2180.
20. Ghasemi Falavarjani K, Habibi A, Anvari P, et al. Effect of segmentation error correction on optical coherence tomography angiography measurements in healthy subjects and diabetic macular oedema. *Br J Ophthalmol*. 2020;104:162–166.
21. Sorour OA, Sabrosa AS, Yasin Alibhai A, et al. Optical coherence tomography angiography analysis of macular vessel density before and after anti-VEGF therapy in eyes with diabetic retinopathy. *Int Ophthalmol*. 2019;39:2361–2371.
22. Lu ES, Cui Y, Le R, et al. Detection of neovascularisation in the vitreoretinal interface slab using widefield swept-source optical coherence tomography angiography in diabetic retinopathy. *Br J Ophthalmol*. In press.